Poole–Frenkel conduction in single wall carbon nanotube composite films built up by electrostatic layer-by-layer deposition

A. S. Jombert,[1,2] K. S. Coleman,[2,a)] D. Wood,[1] M. C. Petty,[1] and D. A. Zeze[1,a),b)]
[1]*School of Engineering and Centre for Molecular and Nanoscale Electronics, Durham University, South Road, Durham DH1 3LE, United Kingdom*
[2]*Department of Chemistry, Durham University, South Road, Durham DH1 3LE, United Kingdom*

(Received 17 May 2008; accepted 9 September 2008; published online 5 November 2008)

The fabrication of large area thin films of single wall carbon nanotubes (SWCNTs) using electrostatic layer-by-layer deposition is reported. The in-plane current versus voltage (*I-V*) characteristics were dependent on the concentration of SWCNTs transferred from the solvents onto the substrates. Solutions with a low SWCNT concentration produced films that exhibited a nonlinear *I-V* regime. The experimental data fitted with various conduction models indicated that Poole–Frenkel conduction was the dominant mechanism. The temperature dependence of the conductivity also supported this model. Two activation energies were identified—approximately 10 and 20 meV. These were thought to be associated with the surfactant coatings of the nanotubes. Increasing the SWCNT loading in the thin films led to an Ohmic conduction process by virtue of a denser network of conductive paths in the film and conduction via tube to tube contacts. © *2008 American Institute of Physics*. [DOI: 10.1063/1.3006015]

I. INTRODUCTION

Carbon nanotubes are very attractive due to their unique electrical and physical properties and also because of their potential for a wide range of applications. These include novel interconnects and nanoelectronic devices such as logic gates[1,2] and memory cells.[3,4] Tasis *et al.*[5] recently published a comprehensive review of nanotube functionalization techniques, developed to address specific applications. While individual nanotubes have been characterized extensively, understanding the basic response (electrical and mechanical) of carbon nanotube composites is still at an early stage, even though polymer-nanotube films are now subjected to a sustained research effort.[6,7]

A very simple method to deposit thin films of noncovalently functionalized nanotubes is the layer-by-layer (LbL) process. This is based on the alternate adsorption of negatively and positively charged species in order to build up multilayer device architectures.[8,9] In LbL deposition, nanometer-thick amorphous polymer shells are formed around individual carbon nanotubes to provide an electrically charged surface; the reversal of the electrostatic charges is then responsible for the build up of multilayers.[10,11] Most of these research initiatives have focused on the chemical modification of the nanotubes. The film structure and electrical response have also been investigated.[6–11] However, the electrical characteristics are often limited to recording the current versus voltage (*I-V*) characteristics, assessing the potential applications, and to reporting the improved conductivity achieved within the polymer composites as a result of the nanotube blending.[6,7] Very little is known about the electrical transport mechanism in the LbL nanotube composites.

This report follows up our previous work[9] and aims to elucidate the conduction process(es) occurring in LbL films of single wall carbon nanotubes (SWCNTs). Monolayers of anionic ($SWCNT_a$) and cationic ($SWCNT_c$) SWCNTs are stacked up as many times as necessary to produce the nanometer-thick devices. The ability to produce large area electrically homogenous ultrathin film composites (thinner than 100 nm) is challenging and of particular interest for applications such as electrochemically active electrodes. Here, the surface morphology of the thin films, their room temperature *I-V* characteristics, and their temperature dependence are reported.

II. THEORY

For Schottky emission, which occurs at the interface between the electrode(s) and the film, the voltage dependence of the barrier energy E is given by the general equation[12]

$$E = E_0 - \frac{n}{2}\left(\frac{e^3}{\pi\varepsilon_0\varepsilon_r}\frac{\eta}{\delta^*}\right)^{1/2} V^{1/2}, \tag{1}$$

where E_0 is the energy at zero field, ε_0 the permittivity of free space, and ε_r the relative permittivity, while e and V are the electronic charge and the applied bias, respectively. The parameters n and η are normally dependent on the type of conduction to be considered. For the Schottky mechanism, n and η are unity. In turn, for the Poole–Frenkel conduction, $n=2$ and η is indicative of the level of the charge for the ionized traps: 1 for singly charged and 2 for doubly charged traps level.[12] The parameter δ^* is the effective electrode separation, and may differ (usually smaller) from the physical electrode separation δ because of the screening effect of the charge carrier accumulation layer(s) at the electrode-film interface.[13] For an in-plane electrode configuration, δ^* will account for the nonuniform distribution of the electrical field between the two electrodes.

a)Authors to whom correspondence should be addressed.
b)Electronic mail: d.a.zeze@durham.ac.uk.

For conductivity dominated by the Schottky effect, the current-voltage dependence may be extracted from Eq. (1)

$$I \propto AT^2 \exp\left(-\frac{E}{kT}\right) = AT^2 \exp\left(-\frac{E_0 - \beta_S V^{1/2}}{kT}\right), \tag{2}$$

where A is the Richardson coefficient, k is the Boltzmann constant, T is the temperature, and β_S is the Schottky coefficient. The following tests may therefore be applied to experimental data to investigate whether or not Schottky conduction is a significant process:[12,14]

(a) Voltage dependence

$$\ln[I/T^2] \propto V^{1/2} \quad \text{or} \quad \ln[I] \propto V^{1/2} \quad \text{(at fixed temperature)}. \tag{3}$$

(b) Temperature dependence

$$\ln[I/T^2] \propto 1/kT \quad \text{(at constant voltage)}. \tag{4}$$

In contrast to Schottky emission, Poole–Frenkel conduction (or field-assisted thermal ionization) is a bulk-limited process in which the conduction is driven by charged traps present within the film.[14,15] In the presence of an electrical field, it also complies with the general voltage dependence of the energy barrier lowering [Eq. (1)] and may be rewritten as

$$E = E_0 - \left(\frac{e^3}{\pi\varepsilon_0\varepsilon_r}\frac{\eta}{\delta^*}\right)^{1/2} V^{1/2} = E_0 - \beta_{\mathrm{PF}} V^{1/2}, \tag{5}$$

where β_{PF}, given by Eq. (6), is the Poole–Frenkel coefficient corrected for the effective electrode separation and the ionization state of the traps contributing to the conduction

$$\beta_{\mathrm{PF}} = 2\beta_S = \beta_0\left(\frac{\eta}{\delta^*}\right)^{1/2} \quad \text{and} \quad \beta_0 = \left(\frac{e^3}{\pi\varepsilon_0\varepsilon_r}\right)^{1/2}. \tag{6}$$

In the Poole–Frenkel conduction model, the current versus voltage dependence,[14,15] equivalent to that of Schottky emission [Eq. (2)], is given by

$$I \propto V \exp\left(-\frac{E_0 - \beta_{\mathrm{PF}} V^{1/2}}{kT}\right). \tag{7}$$

As a result, if this conduction mechanism dominates, then the following equations apply:

(a) Voltage dependence

$$\ln[G] \propto V^{1/2} \quad \text{(at fixed temperature)}. \tag{8}$$

(b) Temperature dependence

$$\ln[I] \propto 1/kT \quad \text{and} \quad \ln[G] \propto 1/kT, \tag{9}$$

where $G(=I/V)$ is the electrical conductance.

III. EXPERIMENT

A. Device architectures

$SWCNT_c$ and $SWCNT_a$ were produced by dispersing the SWCNTs in solutions of dodecyltrimethylammonium bromide (DTAB) and sodium dodecyl sulfate (SDS),[10] respectively. By alternating these cationic and anionic nanotubes, multilayer device architectures were built up using LbL deposition. In practice, a cleaned substrate is dipped into a cationic (or anionic) solution for 30 min to allow the SWCNTs from the solutions to be adsorbed onto the substrate, giving layers of $SWCNT_c$ and $SWCNT_a$. Substrates coated with a $SWCNT_c$ or $SWCNT_a$ layer were subsequently washed with water, dried with nitrogen, and dipped into the counterion solution to form a bilayer. This cyclic process was repeated until the desired device architecture was achieved. Prior to the deposition of the active layer ($SWCNT_c$ or $SWCNT_a$), two or more bilayers of polyelectrolytes (referred to as passive layers) were deposited onto the substrate to enhance the adhesion of the active layers, where polyethylenimine (PEI) and polystyrene sulfonate (PSS) are cationic and anionic polyelectrolytes, respectively.

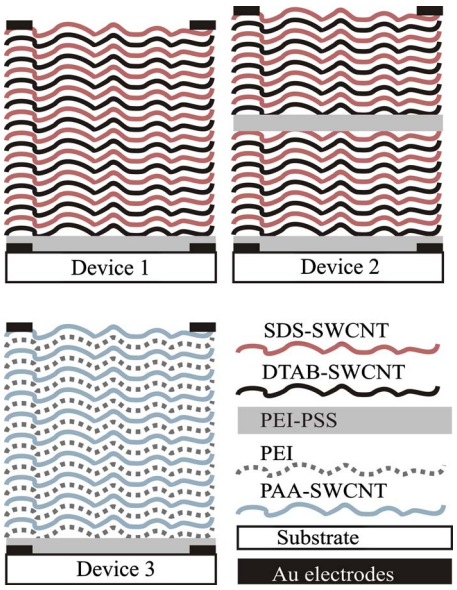

FIG. 1. (Color online) Schematic of the three device architectures of the SWCNT composites fabricated by LbL deposition.

Using the process described above, three device architectures (devices 1–3) were fabricated to investigate the electronic conduction mechanism within the films and to assess the effects of the device configuration on the electrical properties. All three devices contained ten bilayers of $SWCNT_c/SWCNT_a$ or ten bilayers of alternated PEI and polyacrylic acid (PAA) wrapped SWCNTs, [(PEI)/(PAA-SWCNT)], but differed in their arrangement. For instance, the ten $SWCNT_c/SWCNT_a$ bilayers in device 2 were separated in two blocks of five SWCNT bilayers by $[PEI/PSS]_2$. In turn, the $SWCNT_c/SWCNT_a$ was replaced by a [(PEI)/(PAA-SWCNT)] bilayer for device 3. Note that at neutral *p*H in aqueous solutions, PAA is negatively charged.[16,17]

(i) Device 1: $[PEI/PSS]_2[SWCNT_c/SWCNT_a]_{10}$.
(ii) Device 2: $[PEI/PSS]_3[SWCNT_c/SWCNT_a]_5$ $[PEI/PSS]_2[SWCNT_c/SWCNT_a]_5$.
(iii) Device 3: $[PEI/PSS]_2[PEI/PAA\text{-}SWCNT]_{10}$.

Figure 1 illustrates the device architectures. Devices 1 and 1*, which only differed by their SWCNT loading, were used to investigate the effect of SWCNT concentration in the film (Sec. IV D). In turn, devices 1–3 were needed to assess the impact of varying configurations on the magnitude of the

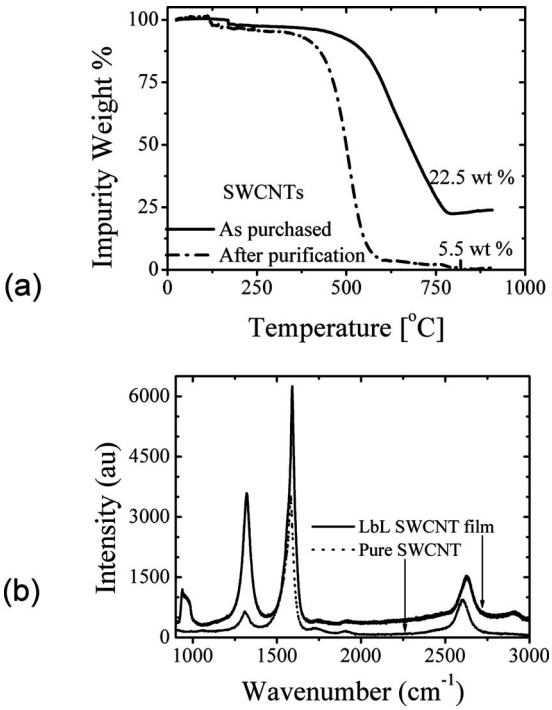

FIG. 2. Thermogravitometric analysis of the purity of the SWCNT used to prepare the (a) LbL films and (b) Raman spectra of the resulting films.

current and the conduction mechanism (e.g., the number of consecutive SWCNT layers required to produce electrically uniform films with a known conduction mechanism).

B. Material preparation

To ensure that the devices are built up from highly purified nanotubes, commercially available SWCNTs (purchased from Carbon Nanotechnologies Inc.) were purified until the metal content was below 5 wt % as shown by the thermogravitometric analysis, Fig. 2(a). In brief, the SWCNTs were subjected to a thermal oxidation for 90 min at 300 °C, followed by stirring in a concentrated HCl bath overnight, before finally rinsing the nanotubes with de-ionized water (until the *p*H of the solution is to that of de-ionized water) and drying overnight at 120 °C.[18,19] The purified SWCNTs were positively and negatively charged by noncovalent surface coatings[8] with SDS and DTAB to produce $SWCNT_a$ and $SWCNT_c$,[9] respectively. Solutions of SDS (1 % wt) and DTAB (0.65 % wt) were prepared by dissolving the surfactants in de-ionized water. The materials produced were analyzed by Raman spectroscopy, Fig. 2(b), to ascertain the presence of SWCNTs in the composites.[9] The relative increase in the sp^3 ($\sim$1350 cm^{-1}) compared to sp^2 band ($\sim$1580 cm^{-1}) in the LbL SWCNT film may have resulted from the surfactant wrapping of the SWCNTs in the matrix.

The following SWCNT concentrations were used:

Device 1: SWCNTs in SDS (0.25 mg/ml) and SWCNTs in DTAB (0.25 mg/ml).
Device 2: SWCNTs in SDS (0.25 mg/ml) and SWCNTs in DTAB (0.25 mg/ml).
Device 3: SWCNTs in SDS (0.1 mg/ml) before PAA wrapping.

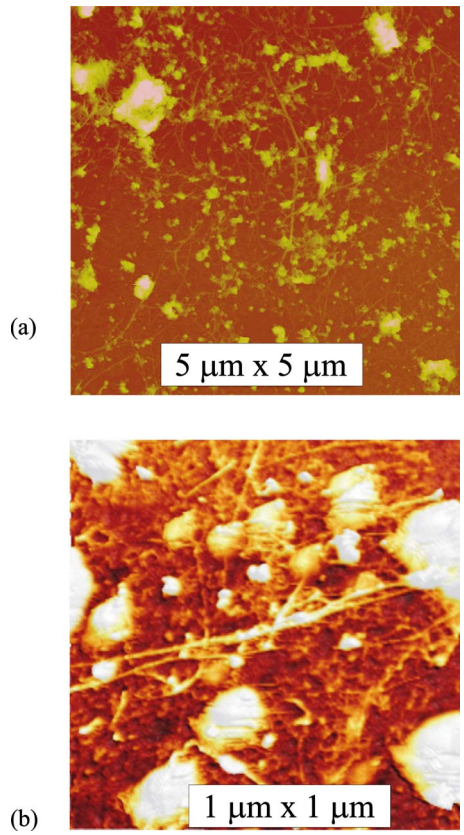

FIG. 3. (Color online) AFM of the surface of the LbL films, (a) 5 $\times$5 μm^2 and (b) 1$\times$1 μm^2, showing individual and bundles of SWCNTs transferred onto the substrate surface for device 1.

Device 1*: SWCNTs in SDS (1.25 mg/ml) and SWCNTs in DTAB (0.82 mg/ml).

In all cases, the solutions were sonicated for about an hour to obtain a homogenous solution, with no apparent (visible) SWCNT clusters. This process allows the clusters to break up into bundles which in turn disperse as individual tubes in the solutions. Figure 3 [atomic force microscopy (AFM) of the surface of the LbL films] showed that individual SWCNTs were transferred onto the substrate surface during deposition and formed a network of SWCNTs within the composites. Figures 3(a) and 3(b) depict a 5$\times$5 μm^2 and a 1$\times$1 μm^2 magnification of the surface topography for device 1, where the lumps (white) seen on the AFM micrographs are believed to be residual surfactant aggregates.

For electrical measurements, glass substrates or oxidized undoped silicon wafers, with prepatterned gold electrodes, were used. The seed layers (PEI/PSS) were deposited onto the prepatterned substrates, while the top Au electrodes were thermally evaporated onto the specimens using a shadow mask. Current-voltage characteristics were recorded by a two-point probe and their temperature dependence was measured from ambient down to 77 K using a liquid nitrogen-based cryostat.

IV. RESULTS AND DISCUSSION

A. Conduction mechanism

The average thickness of the specimens was estimated to be $\sim$70 nm, based on our previously reported experimental

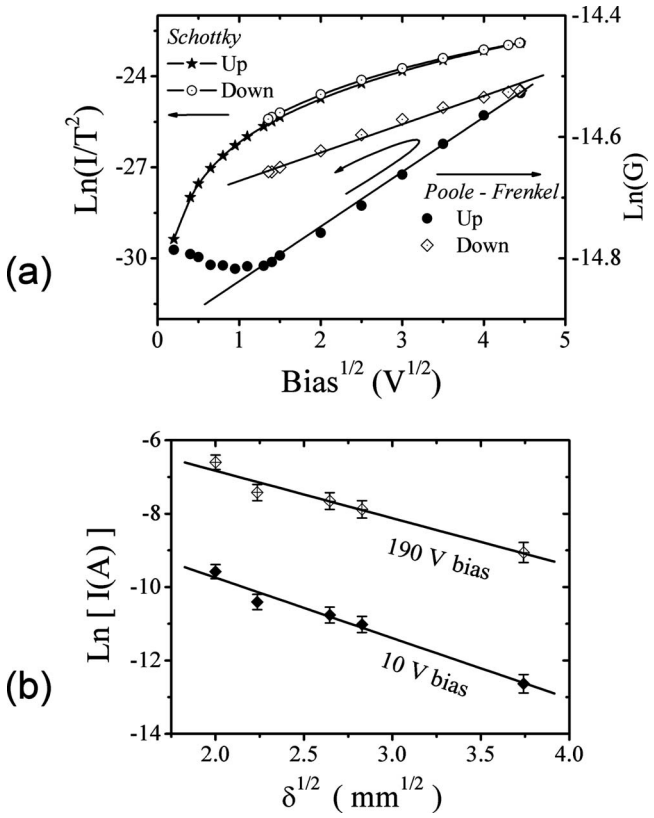

FIG. 4. Current vs voltage characteristics for a device 1 over 0–20 V range. (a) The Schottky emission (left *Y*-axis) and Poole–Frenkel conductivity (right *Y*-axis) plots are shown, likewise (b) the dependence of the current on the electrode separation at 10 and 190 V applied voltages.

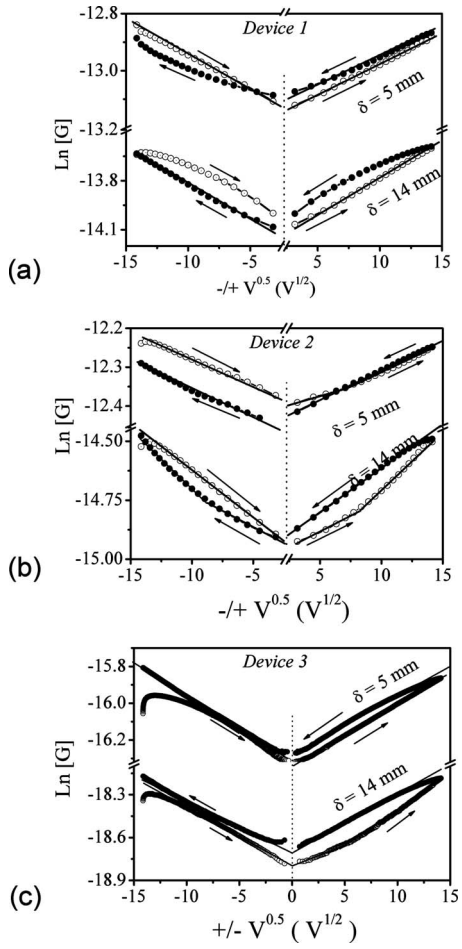

FIG. 5. Comparison of the current vs voltage data, in the form of Poole–Frenkel plots, for (a) device 1, (b) device 2, and (c) device 3 for 5 and 14 mm electrode separations.

data.[9] Figure 4(a) shows the current versus voltage characteristics for a device 1 structure with an electrode separation of 4 mm and over the voltage range of 0–20 V. The data are shown in the forms expected for both Schottky emission [i.e., $\ln(I/T^2)$ versus $V^{0.5}$, Eq. (3)] and Poole–Frenkel conductivity [i.e., $\ln(G)$ versus $V^{0.5}$, Eq. (8)]. It should be noted that a certain degree of hysteresis was found in these measurements, clearly seen for the Poole–Frenkel plot in Fig. 4. Despite this, the Poole–Frenkel model seems to provide a better fit to the experimental data (for both increasing and decreasing voltages above about 1 V) than the Schottky model over a wide variation in current. In Fig. 4(b), the dependence of the current on the electrode separation is explored by plotting the data from a device 1 structure for different electrode separations at applied voltages of 10 and 190 V. The straight lines evident on the $\ln(I)$ versus $\delta^{1/2}$ plot support both the Schottky and Poole–Frenkel models.

Figure 5 compares the current versus voltage data, in the form of Poole–Frenkel plots, for the three device architectures fabricated in this work. The results are shown for two different electrode separations (5 and 14 mm). Reasonably good straight lines are obtained in all cases, in contrast to the Schottky plots [Eq. (3)], which were very nonlinear (data not shown). The hysteresis that is observed, in which the currents measured on increasing the voltage are usually less than those obtained when the voltage is decreased, may possibly result from some charge storage. This hysteresis is consistently present on subsequent voltage scans. Its origin is uncertain and currently under investigation.

Figure 5 reveals that the magnitude of the current in device 2 (current in the microampere range) is somewhat reduced compared to that in device 1 for the 14 mm electrode separation. This is probably the result of the two insulating bilayers of PEI/PSS in the middle of the multilayer architecture. The effect is more marked for device 3 (currents reduced to the nanoampere range) in which a PEI/PAA is interleaved with SWCNT layers. The lower SWCNT content in device 3 may also account for the reduction in the intensity of the current. However, these data suggest that the carbon nanotubes do not penetrate the bilayers of the polyelectrolytes and that the current flow in these multilayer architectures can be confined to the LbL layers containing the SWCNTs.

On a practical note, the devices investigated in this work were all prepared on 75×25 mm^2 glass slides and silicon wafers (51 mm diameter) onto which an ~ 1 μm thick oxide was thermally grown. The fact that the in-plane *I-V* data obey the same conduction model for all the specimens fabricated (devices 1–3) demonstrates that large area films, with a dominant conduction mechanism, can be reproducibly synthesized using LbL techniques.

B. Effective electrode separation

Using ellipsometry measurements at a wavelength of 632 nm, the relative permittivity of our SWCNT LbL films

TABLE I. Correlation between the theoretical and experimental Poole–Frenkel coefficients β_{PF} and the nominal (δ) and effective (δ^*) electrode separation for device 1.

Electrode separation δ (mm)	4	5	8	14
Theoretical β_{PF} (meV cm$^{1/2}$ V$^{-1/2}$)	31.5	28.2	22.3	16.4
Experimental β_{PF} (meV cm$^{1/2}$ V$^{-1/2}$)	36.0	39.0	24.0	21.0
Effective separation δ^* (mm)	2.7	2.3	5.9	8.2

was measured as 2.16 ± 0.02, within the expected range of 2–3 and consistent with a recent report by Eren San *et al.*[20] This value was subsequently used in Eq. (6) to determine the Poole–Frenkel coefficient β_{PF}. Both theoretical (using the measured electrode separations) and experimental (obtained from the slope of the $\ln(G)$ versus $V^{0.5}$ graphs) values of β_{PF} (with $\beta_0 = 5.16 \times 10^{-5}$ eV m$^{1/2}$ V$^{-1/2}$), together with the value of the effective electrode separation δ^*, are compared in Table I. The δ^* values were obtained using $\eta = 2$ to account for the cationic and anionic charges of the surfactants (traps) contributing to the conduction.

Analysis of the electrical data for all of the samples studied revealed that the effective electrode separation decreased with the number of consecutive SWCNT layers in direct contact with the electrodes, with an average of $\delta^*/\delta \approx 0.9$, 0.6, and 0.5 obtained for device 1 (ten bilayers), device 2 (five bilayers), and device 3 (one layer), respectively. This implies a varying degree of homogeneity of the electrical field across the films. The device configuration and the connectivity between conductive paths within the composites (i.e., concentration of SWCNTs in the composite and how they are dispersed across the substrate) may explain the reduction in the effective electrode separation with the numbers of consecutive active layers. The surfactant layer interleaved between consecutive layers reduces volume conductivity, so confining the conduction within the consecutive active layers in direct contact with the electrodes.

C. Temperature dependence

If Poole–Frenkel conductivity dominates in our samples, then the temperature dependence of the conductance should be given by Eq. (9), i.e.,

$$\ln[G] \propto \frac{1}{kT} \quad \text{or} \quad \Delta \ln[G] = \frac{\Delta E}{kT} = -(E_0 - \beta_{PF} V^{1/2}) \frac{1}{kT}, \tag{10}$$

where ΔE represents an activation energy.

Figure 6 shows $\ln[G]$ versus T^{-1} data for a device 2 architecture at a constant applied bias of 10 and 100 V. In each case, reasonable straight lines are evident above and below a transition temperature of about 155 K. Such transition temperatures are particularly useful to determine the relationship between dominant densities of state.[21] Attempts to fit the same data to the Schottky model [Eq. (4)] produced very poor fits (data not shown). Devices 1 and 3 structures exhibited very similar temperature data and will not be discussed in detail here. Mathew *et al.*[12] attributed the variation in the slope above and below the transition temperature to

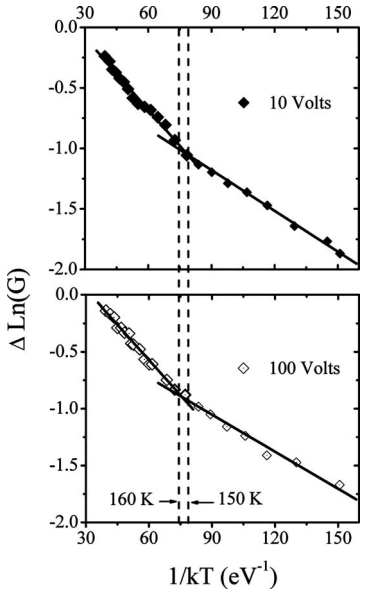

FIG. 6. Temperature dependence of the conductance for our LbL films at (a) 10 and (b) 100 V, with the corresponding activation energy ΔE given in Table II.

the presence of at least two trap levels. Although this conclusion was drawn investigating Poole–Frenkel conduction in CdTe and Mo–Cu_2O, it is consistent with the presence of cationic and anionic surfactants (potential traps) within the LbL SWCNT film matrix. Well defined activation energies may be identified in different temperature regions if the carrier mobility of the density of states is affected differently by the temperature within the range considered. Temperature-induced changes in activation energies are well documented[21] and will not be discussed further.

The activation energy values did not vary significantly between the data obtained at 10 V and 100 V (Fig. 6). However, the figure for ΔE above the transition temperature ($\sim$20 meV) was approximately twice that below the transition temperature ($\sim$10 meV). The various activation energies obtained from the data in Fig. 6 are given in Table II. These are of the same order with those reported by Choi *et al.*[22] who found 12.2 and 1.4 meV in boron- and nitrogen-doped SWCNT mats, respectively. However these values are low compared with the activation energy for individual B-doped nanotubes, reported to be 55–70 meV.[23] It is also believed that the number of SWCNTs effectively transferred above the percolation threshold is another factor that contributes to lowering of the activation energy as a greater connectivity and near-uniform coverage of SWCNTs across the substrate increase the effective electrical field. The values of the activation energies (a few meV) suggest that only shallow

TABLE II. Variation in the activation energy for device 2 calculated using the slopes of $\ln(G)$ vs $1/kT$, from room temperature to 77 K.

	Activation energy ΔE (meV)	
Bias	$T > 155$ K	$T < 155$ K
10 V	19.9	11.2
100 V	21.9	10.9

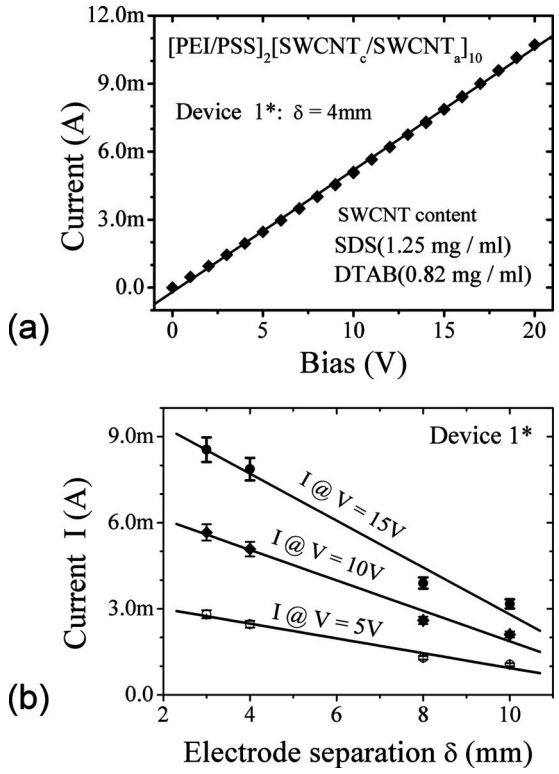

FIG. 7. (a) Current vs voltage and (b) current vs electrode separation for device 1*.

traps are involved in the LbL SWCNT composites synthesized, attributable to the presence of surfactants shells around the nanotubes.

D. Effect of nanotube loading

The effect of the concentration of SWCNTs in the composites was investigated using a modified device 1 architecture. Device 1* was therefore produced from solutions of SDS and DTAB containing at least three times more SWCNTs than those for devices 1, 2, and 3, as described in the Sec. III. Figure 7 shows the current versus voltage [Fig. 7(a)] and the current versus electrode separation [Fig. 7(b) results for device 1*, all of which exhibit a linear dependence. Note that no hysteresis was observed for device 1*. The current level is three orders of magnitude higher than that measured for device 1, reflecting the higher SWCNT content in the multilayer architecture. The results also suggest that a simple Ohmic conduction process is sufficient to account for the electrical conductivity.

A model of conduction within our LbL SWCNT composites is shown in Fig. 8. Two types of conductive path are depicted. In the first, C_1 or C_2, the conduction is limited by the voltage drop across the outer (surfactant) coating of the functionalized SWCNTs (C_1:SWCNT$_c$-SWCNT$_a$ and C_2:SWCNT-SWCNT$_{a/c}$ contacts). This accounts for the Poole–Frenkel conductivity observed in the device configurations (devices 1–3) reported earlier in this paper. The trapping levels are therefore those associated with the surfactant coatings. The other kind of conduction path C_3 results from tube to tube contact. This will dominate for high nanotube concentrations and accounts for the Ohmic behavior of device 1*. However, despite the dominance of Poole–Frenkel conduction in devices 1–3, tunneling, tube to tube hopping, interface electrodes, and conduction through the polyelectrolyte shells should not be completely discounted. Tunneling[14] may also occur between two adjacent sites if the thickness of the insulator separating them is extremely thin (below 50 Å). Equally, intertube hopping[24] may exist between stack of individual uncoated SWCNTs.

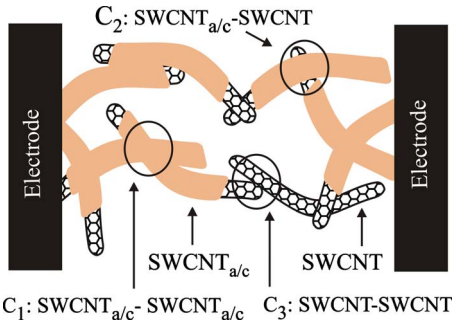

FIG. 8. (Color online) A proposed model of conduction within our LbL SWCNT composites, depicting the two types of conductive paths: (i) C_1:SWCNT$_c$-SWCNT$_a$ and C_2:SWCNT-SWCNT$_{a/c}$ contacts and (ii) C_3: SWCNT-SWCNT contacts.

V. CONCLUSIONS

Large area of SWCNT thin film composites have been produced using the LbL deposition process. At room temperature, the in-plane conduction was dependent on the amount of SWCNTs transferred effectively from the solution onto the substrates. While an Ohmic conduction was observed in films having a higher SWCNT concentration, the conduction in composites with a lower SWCNT loading was driven by the Poole–Frenkel mechanism, which was also independent of the precise device configuration and the magnitude of the electrode separations up to 14 mm. The temperature (293–77 K) dependence of the conductance provided a further confirmation of the dominance of the Poole–Frenkel mechanism. Furthermore, a transition temperature observed between ~150 and 160 K indicated that two levels of ionized traps contributed to conduction. These were believed to result from the presence of the anionic and cationic surfactant shells around the nanotubes. A simplified model, based on the SWCNT loading, tube to tube contacts, and contacts between functionalized tubes, was proposed to explain the electrical behavior of the films produced.

ACKNOWLEDGMENTS

The authors would like to thank the Engineering and UK Physical Sciences Research Council (EPSRC-GB, DTA studentship) and Regional Development Agency, One North-East (Grant No. SP 082), for the financial support.

[1]S. Iijima, Nature (London) **354**, 56 (1991).
[2]Z. Chen, J. Appenzeller, Y.-M. Lin, J. Sippel-Oakley, A. G. Rinzler, J. Tang, S. J. Wind, P. M. Solomon, and P. Avouris, Science **311**, 1735 (2006).
[3]J. W. Kang and Q. Jiang, Nanotechnology **18**, 095705 (2007).
[4]A. Star, Y. Lu, K. Bradley, and G. Gruner, Nano Lett. **4**, 1587 (2004).
[5]D. Tasis, N. Tagmatarchis, A. Bianco, and M. Prato, Chem. Rev. (Wash-

ington, D.C.) **106**, 1105 (2006).
[6]V. Bliznyuk, S. Singamaneni, M. Atashbar, and R. Kattumenu, Appl. Phys. Lett. **88**, 164101 (2006).
[7]S. P. Lee, H. Choi, K. W. Lee, K. H. Mo, J. W. Jang, E. Lee, I.-M. Kim, and C. E. Lee, J. Korean Phys. Soc. **48**, 146 (2006).
[8]M. Zhang, L. Su, and L. Mao, Carbon **44**, 276 (2006).
[9]M. Palumbo, K. U. Lee, B. T. Ahn, A. Suri, K. S. Coleman, D. Zeze, D. Wood, C. Pearson, and M. C. Petty, J. Phys. D **39**, 3077 (2006).
[10]G. Decher, Science **277**, 1232 (1997).
[11]A. A. Mamedov, N. A. Kotov, M. Prato, D. M. Guldi, J. P. Wicksted, and A. Hirsch, Nature Mater. **1**, 190 (2002).
[12]X. Mathew, J. P. Enriquez, P. J. Sebastian, M. Pattabi, A. Sanchez-Juarez, J. Campos, J. C. McClure, and V. P. Singh, Sol. Energy Mater. Sol. Cells **63**, 355 (2000).
[13]J. J. Mares, J. Kristofik, V. Smid, and F. Deml, Solid-State Electron. **31**, 1309 (1988).
[14]S. Senthilarasu, R. Sathyamoorthy, S. Lalitha, and A. Subbarayan, Sol. Energy Mater. Sol. Cells **90**, 783 (2006).
[15]P. V. Aleskandrova, V. K. Gueorguiev, Tz. E. Ivanov, and J. B. Koprinarova, Eur. Phys. J. B **52**, 453 (2006).
[16]A. Liu, T. Watanabe, I. Honma, J. Wang, and H. Zhou, Biosens. Bioelectron. **22**, 694 (2006).
[17]M. O'Connell, P. Boul, L. Ericson, C. Huffman, Y. Wang, E. Haroz, C. Kuper, J. Tour, and K. D. Ausman, Chem. Phys. Lett. **342**, 265 (2001).
[18]H.-T. Fang, C.-G. Liu, F. Li, M. Liu, and H.-M. Cheng, Chem. Mater. **16**, 5744 (2004).
[19]S. Gajewski, H. E. Maneck, U. Knoll, D. Neubert, I. Dorfel, R. Mach, B. Strauss, and J. F. Friedrich, Diamond Relat. Mater. **12**, 816 (2003).
[20]S. Eren San, Y. Yerli, M. Okutan, F. Yılmaz, O. Gunaydın, and Y. Hames, Mater. Sci. Eng., B **138**, 284 (2007).
[21]G. G. Roberts, Phys. Rep. **60**, 59 (1980).
[22]Y.-M. Choi, D.-S. Lee, R. Czerw, P.-W. Chiu, N. Grobert, M. Terrones, M. Reyes-Reyes, H. Terrones, J.-C. Charlier, P. M. Ajayan, S. Roth, D. L. Carroll, and Y.-W. Park, Nano Lett. **3**, 839 (2003).
[23]B. Q. Wei, R. Spolenak, P. Kohler-Redlich, M. Ruhle, and E. Arzt, Appl. Phys. Lett. **74**, 3149 (1999).
[24]T. Fukao, S. Nakamura, H. Kataura, and M. Shiraishi, Jpn. J. Appl. Phys., Part 1 **45**, 6524 (2006).